/
## Article / Book Information

| | |
|---|---|
| Title | Large Torsion Thin Artificial Muscles Tensegrity Structure for Twist Manipulation |
| Authors | Ryota Kobayashi, Hiroyuki Nabae, Koichi Suzumori |
| Citation | IEEE Robotics and Automation Letters, Volume 8, Issue 3, pp. 1207-1214 |
| Pub. date | 2023, 1 |
| Copyright | (c) 2023 IEEE. Personal use of this material is permitted. Permission from IEEE must be obtained for all other uses, in any current or future media, including reprinting/republishing this material for advertising or promotional purposes, creating new collective works, for resale or redistribution to servers or lists, or reuse of any copyrighted component of this work in other works. |
| DOI | https://dx.doi.org/10.1109/LRA.2023.3236889 |
| Note | This file is author (final) version. |

# Large Torsion Thin Artificial Muscles Tensegrity Structure for Twist Manipulation

Ryota Kobayashi[1], Hiroyuki Nabae[1], and Koichi Suzumori[1]

*Abstract*—Tensegrity structures have been actively studied in recent years because they are lightweight, compliant, and flexible, which are properties not typically found in conventional robots. This structure can be modularized to create soft robots that operate in unknown environments such as cave or space with more complex and effective behavior. The basic deformation elements in modularization are stretching, bending, and torsion. Among them, torsional motion is important for proper manipulation and rotational operation. However, active, and large torsion in soft tensegrity structures has not been developed. Therefore, this study describes torsional deformation and a novel arrangement method for thin artificial muscles. The proposed method leads to the optimal placement of artificial muscles for torsion, by which we generated a large torsion of $\pm 50$ deg. This is more than 2.5 times larger than that of a previous tensegrity without compromising the favorable properties of the structure. Furthermore, by modularizing the tensegrity structure, a tensegrity arm capable of removing a plastic bottle cap was developed. The applicability of torsional deformation and the usefulness of modularization of the structure are demonstrated.

*Index Terms*—Soft robot applications, Tensegrity structure, Torsion, Thin McKibben muscle



Fig. 1. Soft tensegrity robot with multiple DOFs that consists of several six-bar tensegrity modules and can operate in an unknown environment.

## I. INTRODUCTION

TENSEGRITY is a structure consisting of tension and compression members, and it has unique characteristics not found in other structures [1]. Tensegrity structures have been used in a variety of fields, including architecture [2] that takes advantage of their strength-to-weight ratio and art [3] that takes advantage of their high scalability. In recent years, in addition to these excellent properties, the environmental adaptability derived from the softness of the soft tensegrity has been focused, and tensegrity robots were developed in the field of robotics [4], [5], [6]. Tensegrity robots are expected to play an active role not only in cooperative work with humans [7], which has been done by conventional robots, but also in dangerous work in unknown spaces such as caves [8] and outer space [9], owing to their environmental adaptability, scalability, and high durability. To realize high functionality of soft tensegrity robots in such environments, modularization is effective in terms of versatility [10], [11], and it is desirable to be able t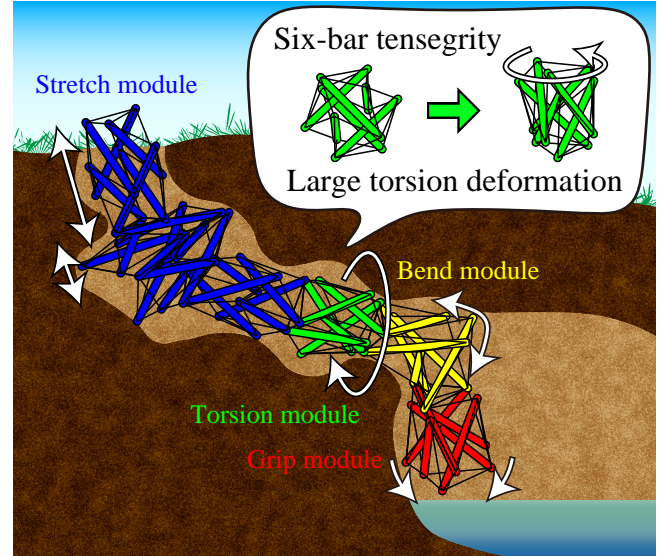o perform various deformations in a single module. Therefore, it is important to determine which tensegrity structure can be modularized as a single module.

A wide variety of configurations are used for tensegrity robots, including prisms [12], six-bar tensegrity [9], 12-bar rhombicuboctahedron [13], and spine-like shapes [14]. The six-bar tensegrity shown in Fig. 1 has a simple structure and is easy to construct. It also has a higher symmetry and degrees of freedom (DOFs) than the simplest prismatic structure that consists of three struts. Therefore, six-bar tensegrity can form the basic structure of a robot module with high functionality that can achieve large deformations of basic deformation modes, such as stretching, bending, and torsion, similar to elements of living organisms. Although considerable research has been conducted using six-bar tensegrity [9], [15], [16], the deformation of tensegrity structures in these robots is limited to a small stretching deformation. Most robot movements are passive due to gravity and limited to rolling motions, which is not suited for performing a variety of active tasks in an unknown spatial configuration.

Furthermore, it is difficult to fully utilize the lightness and flexibility of tensegrity structures, especially soft tensegrity structures with rubber threads, when hard and heavy actuators such as electromagnetic motors and cylinders are used [9]. A method using thermally driven artificial muscles [17] has also been suggested; however, it presents difficulties related to long thermal response.

In this study, we aim to develop a multi-DOF soft tensegrity

[1]Ryota Kobayashi, Hiroyuki Nabae, and Koichi Suzumori are with the Department of Mechanical Engineering, Tokyo Institute of Technology, 2-12-1 Ookayama, Meguro-ku, Tokyo 152-8550, Japan `kobayashi.r.at@m.titech.ac.jp`

Digital Object Identifier (DOI): see top of this page.

robot, with high adaptability to the environment and the ability to accomplish various tasks by developing a tensegrity module capable of handling various large deformations (Fig. 1).

Previously, we developed an inchworm-type robot that moves with large deformations of its tensegrity structure to explore unknown spaces [8]. This robot used six-bar tensegrity and thin McKibben muscles [18], and was comprised of a tensegrity module with displacements of 20%–40% in the axial and radial directions. Additionally, in [11], we produced a robotic hand with large bending deformations by combining a hand-type structure with a tensegrity module and thin McKibben muscles. The use of thin McKibben muscles retains the light weight of normal McKibben muscles [19], but also allows for deformation without losing the characteristics of the soft tensegrity structure, because of its flexibility to be driven even in a bent state [8], [11], [20]. By adding torsional motion which is important for proper manipulation and rotational operation to the above mentioned approach, all basic deformation modes of the module can be realized, and the development of a versatile tensegrity robot with even greater applicability is expected.

However, to the best of our knowledge, no studies have achieved torsional deformation in the six-bar tensegrity. In other tensegrity structures, there are only a few studies on torsion compared to stretching and bending, and the amount of deformation is less than 20 deg per stage [21], [22], [23]. Furthermore, it is unsuitable for the purposes of this study because it uses a tensegrity structure with low symmetry, which makes it difficult to combine other deformation modes, and does not have axial flexibility [21], [22] or passive torsional motion in response to external forces [23], [24]. Here, internal force means that the actuator is complete within a single tensegrity. The robot we are aiming for, as shown in Fig. 1, must be able to adapt to its environment in an unknown space and perform active tasks, so it is necessary to realize active deformation, which has never been studied before in soft tensegrity.

Therefore, this paper proposes a novel method to achieve large torsional deformation in a tensegrity module by combining six-bar tensegrity and thin McKibben muscles. In this method, the distance between the vertices of two struts is varied using thin artificial muscles, and torsion is induced by significantly disrupting axial symmetry. Furthermore, to prevent interference in operation when combined with other deformation modes, the design excludes bending deformation and minimizes the axial length change. As an example of modularization, a tensegrity arm was developed by combin-
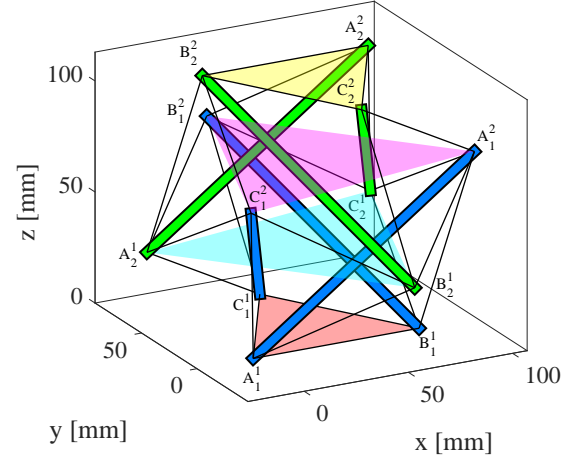


Fig. 2. Six-bar tensegrity used in this study with names and set variables for tensegrity vertices.

ing tensegrity structures with several functions. This study describes an experiment to remove a plastic bottle cap to display the operability of this tensegrity arm. The modularized tensegrity arm is compared with other tensegrity arms in Table I. The main advantage of our approach is that it is the first to combine both internally driven motion and independent deformation modules.

The remainder of this paper is organized as follows. In Section II, the concept of torsional deformation of tensegrity structures is explained, and a tensegrity structure with torsional deformation is designed. Section III describes the design and operational experiments of a robot arm with a torsionally deformable tensegrity structure as a module. Finally, conclusions and future plans are presented in Section IV.

## II. DESIGN OF TORSIONAL TENSEGRITY

The tensegrity used in this study is a soft structure with various deformation possibilities. It is difficult to induce torsional deformation without other deformation elements, as is the case with large bending deformation in the torsion of [24]. This section describes a method to induce torsional deformation in tensegrity and optimizes the arrangement of artificial muscles to minimize contraction and bending deformations to achieve torsional deformation.

### A. New Muscle Arrangement for Torsional Tensegrity

The six-bar tensegrity consists of four layers, as shown by the four colors in Fig. 2, The layer containing triangle $A_1^1B_1^1C_1^1$

TABLE I
COMPARISON OF TENSEGRITY ROBOT ARMS.

| Robot | Actuators | Force type | Deformation elements | Deformation elements are independent or not | References |
|---|---|---|---|---|---|
| Tensegrity arm of this paper | Thin McKibben muscles | Internal | Stretch and Torsion | Yes | – |
| New Soft Robot Hand | Thin McKibben muscles | External | Bend | – | [11] |
| HEDRA | Stepper motors | External | Stretch, Bend, and Torsion | No | [24] |
| Bio-Inspired Tensegrity Manipulator | DC motors | External | Bend | – | [25] |
| Modular Tensegrity Robot Arm | Pneumatic cylinders | Internal | Bend | – | [26] |
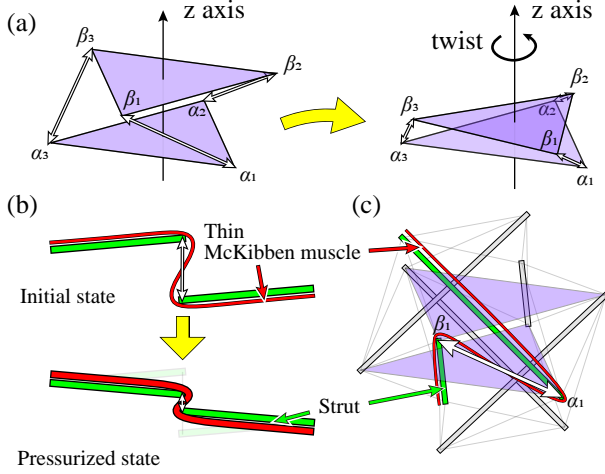
Fig. 3. (a) Torsional deformation between triangles due to proximity between two points. (b) Method for achieving proximity between two points. (c) Achieving the deformation in (a).

is the 1st layer, the layer containing triangle $A_2^1 B_2^1 C_2^1$ is the 2nd layer, the layer containing triangle $A_1^2 B_1^2 C_1^2$ is the 3rd layer, and the layer containing triangle $A_2^2 B_2^2 C_2^2$ is the 4th layer. Using these layers, torsional deformation of the tensegrity structure was considered.

First, torsion of the tensegrity structure around the z-axis indicates that torsion occurred between the triangles in the 1st and 4th layers. If the entire structure is torsionally twisted around the z-axis, torsion occurs between the triangles in each layer. Therefore, it is believed that the entire tensegrity structure can be torsioned by inducing torsional deformation between the triangles in each layer.

As shown in Fig. 3(a), bringing the vertices of the two triangles closer together causes a twist between them. The approach distance between the two vertices, as shown in Fig. 3(a) can be obtained using the artificial muscle arrangement shown in Fig. 3(b) using the artificial muscles proposed in this study. Artificial muscles are suitable actuators for bringing these two points closer together. However, because the contraction ratio of the artificial muscle is approximately 20%, even if $\alpha_1$ and $\beta_1$ shown in Fig. 3(a) are connected by an artificial muscle, a large twist is not expected. The method shown in Fig. 3(b) is an effective method for increasing the contractile performance between two points. As shown in Fig. 3(b), one artificial muscle is placed via two struts, whose vertices are the two points to be approached. Because the length of the strut was invariant, the contraction of the artificial muscle translates into an approach between two points. Therefore, artificial muscles were placed, as shown in Fig. 3(c) to bring $\alpha_1$ and $\beta_1$ closer together, and similarly between $\alpha_2$ and $\beta_2$, and between $\alpha_3$ and $\beta_3$, to achieve a twist between the triangles shown in Fig. 3(a). In this study, a method of placing three artificial muscles to create a twist between two triangles, such that $\alpha_1$ and $\beta_1$ are brought closer together is denoted as $[\alpha_1 \leftrightarrow \beta_1]$. This novel method takes advantage of the ability of thin artificial muscles to be driven in a bent state, and it is thought that this method can be used to achieve a twist deformation without compromising its inherent advantageous

properties, such as tensegrity lightness and flexibility.

The tensegrity structure consists of four layers of triangles, which can be divided into two pairs. Torsion can be generated in the structure by combining the twists of the triangles in each pair. Both the method of dividing the four triangles into two pairs and that of placing artificial muscles are optimized to maximize the torsion angle in Section II-C.

### B. Kinematics and Statics for Torsional Tensegrity

An artificial muscle is an actuator whose load varies with its length. Therefore, in addition to conventional tensegrity analysis [27], [28], it is necessary to consider the force characteristics of the artificial muscle. The kinematics and statics of deforming a tensegrity structure in the z-axis and radial directions using artificial muscles are described in [8]. However, [8] only considered the case of extension and contraction in the z-axis direction, and it was not possible to analyze the mechanics considering torsional deformation around the z-axis direction. Therefore, in this study, new variables were set to consider the torsional deformation of tensegrity, and a static analysis was conducted using these variables, considering the loads on the rubber threads and artificial muscles.

The names of the vertices in the tensegrity structure is shown in Fig. 2, and the strut length is denoted by $L$. The set of struts containing the vertex represented by $X_1^i$ in the tensegrity structure is denoted as Structure I, and the set of struts containing the vertex represented by $X_2^i$ is denoted as Structure II. In this study, 12 vertices are represented by eight variables, $r_1$, $\theta_1$, $\phi_1$, $r_2$, $\theta_2$, $\phi_2$, $h$, and $\psi$, such that torsional deformation can be considered. The following section describes how the variables are set and the coordinates of each vertex is obtained using these variables. In this paper, the position vector of vertex $X_i^j$ is described as $\boldsymbol{X}_i^j$.

First, by expressing the inclination of the strut using $\theta_1, \phi_1$, the position of strut $A_1^1 A_1^2$ is determined as Eqs. (1) and (2). The angle $\theta_1$ is the polar angle of $\boldsymbol{A}_1^2 - \boldsymbol{A}_1^1$ and $\phi_1$ is the azimuth angle of $\boldsymbol{A}_1^2 - \boldsymbol{A}_1^1$.

$$\boldsymbol{A}_1^1(r_1, \theta_1, \phi_1) = (0,\ 0,\ 0)^\top, \tag{1}$$

$$\boldsymbol{A}_1^2(r_1, \theta_1, \phi_1) = \begin{pmatrix} L \sin\theta_1 \cos\phi_1 \\ L \sin\theta_1 \sin\phi_1 \\ L \cos\theta_1 \end{pmatrix}. \tag{2}$$

Then, with $r_1$ as the length of one side in the bottom triangle of the tensegrity structure and $h$ as its height, $\boldsymbol{P}(r_1)$, the center of the tensegrity structure for Structure I, is expressed as in Eq. (3).

$$\boldsymbol{P}(r_1) = \left( \frac{1}{2} r_1,\ \frac{\sqrt{3}}{6} r_1,\ \frac{h}{2} \right)^\top \tag{3}$$

The coordinates of the remaining vertices of Structure I were obtained by rotating $\boldsymbol{A}_1^1, \boldsymbol{A}_1^2$ around an axis that passes through $\boldsymbol{P}(r_1)$ and is parallel to the z-axis. In other words, with $i = 1, 2$, the following is obtained:

$$\boldsymbol{B}_1^i(r_1, \theta_1, \phi_1) = \boldsymbol{R}_z\left(\frac{2}{3}\pi\right)\left(\boldsymbol{A}_1^i - \boldsymbol{P}(r_1)\right) + \boldsymbol{P}(r_1), \tag{4}$$

$$\boldsymbol{C}_1^i(r_1, \theta_1, \phi_1) = \boldsymbol{R}_z\left(\frac{4}{3}\pi\right)\left(\boldsymbol{A}_1^i - \boldsymbol{P}(r_1)\right) + \boldsymbol{P}(r_1). \tag{5}$$

Note that $\boldsymbol{R}_z(\theta)$ is a rotation matrix that rotates $\theta$ around the z-axis. The method used to obtain the coordinates of Structure II is as follows. (i) First, the parameters $r_1, \theta_1$, and $\phi_1$ in Structure I are replaced by $r_2, \theta_2$, and $\phi_2$. So, $\theta_2$ is the polar angle of $\boldsymbol{A}_2^1 - \boldsymbol{A}_2^2$, $\phi_2$ is the azimuth angle of $\boldsymbol{A}_2^1 - \boldsymbol{A}_2^2$ at this time and $r_2$ is the length of one side in the top triangle of the tensegrity structure. And each vertex are moved using symmetry with respect to P($r_2$). The position vector of P($r_2$) can be obtained by replacing $r_1$ in Eq. (3) with $r_2$. (ii) Each point is rotated $\psi$ around an axis that passes through P($r_2$) and is parallel to the z-axis. So, $\psi$ is a variable used to describe the torsion angle of the tensegrity structure. (iii) Each vertex of Structure II is translated by $\boldsymbol{P}(r_2) - \boldsymbol{P}(r_1)$, such that the centers P($r_1$) and P($r_2$) of the tensegrity structures for Structures I and II are aligned. By combining (i) to (iii) into one formula, all vertices of Structure II are obtained, as in (6). Note that $\boldsymbol{X} = \boldsymbol{A}, \boldsymbol{B}, \boldsymbol{C}$ and $i = 1, 2$.

$$\boldsymbol{X}_2^i = \boldsymbol{R}_z(\psi)\left\{\boldsymbol{P}(r_2) - \boldsymbol{X}_1^{3-i}(r_2, \theta_2, \phi_2)\right\} + \boldsymbol{P}(r_1) \quad (6)$$

Using the variables described above, it is possible to conduct a static analysis of a tensegrity structure by considering torsional deformation.

A static analysis was conducted in the same method which is described in [8] and is based on the potential energy without noise or disturbance. Because the artificial muscles were the same as those used for the robot described in [8], the same values were used for the force characteristics. However, because the rubber threads that compose the tensegrity structure have different diameters from those used for the robot described in [8], the load on the rubber threads were measured again. Figure 4 shows the load on the rubber thread with respect to the rubber thread length, which is normalized by the natural length of the rubber thread. The change in load was recorded while the rubber thread was stretched from its natural length to a sufficient length and then returned to its natural length. Hysteresis between the load and the rubber thread length was observed, and the arrows in Fig. 4 indicate the order of data acquisition. The least-squares method was used to approximate the relationship between the load $f(l_{\text{rubber}})$ of the rubber thread and length $l_{\text{rubber}}$ as a 12th order function. When the load of rubber thread is got, the maximum order of the approximation function was determined based on the minimum value for which the norm of the error vector was less than 1% of the measured maximum load in [8], so the same method was used here. In this case, the total potential energy of the tensegrity structure is obtained using (7).

$$U(r_1, \theta_1, \phi_1, r_2, \theta_2, \phi_2, h, \psi) = \sum_{\text{all}} F + \sum_{\text{all}} G, \quad (7)$$

where $\sum_{\text{all}} F$ is the total potential energy of the rubber threads and $\sum_{\text{all}} G$ is the total potential energy of the artificial muscles. The placement of these artificial muscles is based on the novel method shown in Fig. 3. The partial differentiation of this energy by the eight variables yields the following
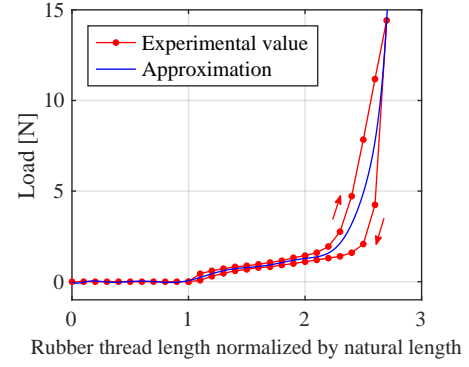


Fig. 4. Load on the rubber thread used in the tensegrity structure with respect to its rate of change in length.
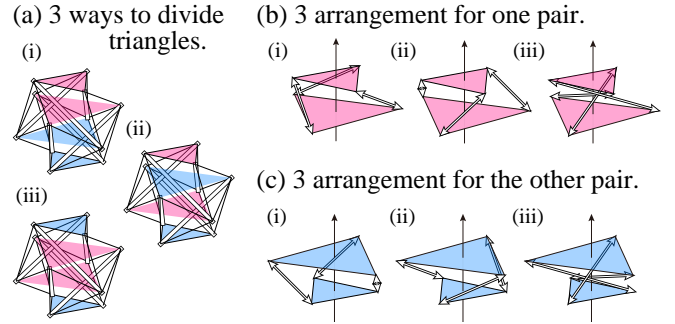


Fig. 5. (a) Three ways to divide the four triangles into two pairs. Three methods to place artificial muscles between (b) red, and (c) blue triangles. Considering (a), (b), and (c), there are $3 \times 3 \times 3 = 27$ placement methods of the artificial muscles.

equations for the balance of forces:

$$\frac{\partial U}{\partial r_1} = 0, \ \frac{\partial U}{\partial \theta_1} = 0, \ \frac{\partial U}{\partial \phi_1} = 0, \ \frac{\partial U}{\partial r_2} = 0,$$
$$\frac{\partial U}{\partial \theta_2} = 0, \ \frac{\partial U}{\partial \phi_2} = 0, \ \frac{\partial U}{\partial h} = 0, \ \frac{\partial U}{\partial \psi} = 0. \quad (8)$$

The torsional deformation of the tensegrity structure can be calculated by solving these equations.

### C. Optimization by Numerical Simulation

Four-layered tensegrity triangles were divided into two pairs. For each pair, the method shown in Fig. 3 was used to twist the triangles, as shown in Fig. 3(a). There are three ways to divide the four triangles into two pairs by considering the pair that includes the first layer as shown in Fig. 5(a). There are three methods to place artificial muscles between the two triangles as shown in Figs. 5(b) and 5(c). This is because in Fig. 3(a), there are three possible points at which $\alpha_1$ can be brought into proximity: $\beta_1$, $\beta_2$, and $\beta_3$. Therefore, there are $3 \times 3^2 = 27$ possible arrangements of artificial muscles that could cause the tensegrity structure to torsion around the z-axis by considering the division of the four triangles and the twisting of each triangle with respect to the others. Tensegrity structures are extraordinarily complex, and deformation is difficult to estimate because it is determined by the balance between the elastic forces of all the rubber bands and the loads of all the artificial muscles. Therefore, simulations were conducted to determine the optimal placement of the artificial

muscles to generate torsion in the tensegrity, by simulating all 27 placement methods of the artificial muscles. In addition to the torsion angle, it is important to avoid other deformation factors such as stretching and bending. It is easy to generate only passive torsion by providing a height constraint by an external force. However, the goal here is to achieve active torsion using artificial muscles. Therefore, there is no constraint in the height direction of the soft tensegrity, and depending on the placement of the artificial muscles, contraction or bending may occur along with the torsion. However, bending does not occur with the used placement method; therefore, the placement method of the artificial muscles was optimized by considering the amount of change in the height direction of the structure.

Here, a simulation method for the deformation of tensegrity using artificial muscles is described. First, the strut length of the tensegrity structure $L$ was 130 mm, and the natural length of the rubber thread was 60 mm. The following is an example of placing artificial muscles at $[A_1^1 \leftrightarrow A_2^1]$ and $[A_1^2 \leftrightarrow C_2^2]$: In this study, the method of placing artificial muscles is denoted as "$\left(A_1^1 A_2^1,\ A_1^2 C_2^2\right)$." In this case, there were six artificial muscles in the tensegrity structure: three artificial muscles have the same lengths as $\left|A_1^1 A_2^1\right| + 2L$ in the initial state (Fig. 2) and the other three artificial muscles have the same lengths as $\left|A_1^2 C_2^2\right| + 2L$ in the initial state. The potential energy, $\sum_{\text{all}} G$ of the artificial muscles in (7) can be expressed as follows:

$$\sum_{\text{all}} G = 3G\left(2L + \left|A_1^1 A_2^1\right|\right) + 3G\left(2L + \left|A_1^2 C_2^2\right|\right). \quad (9)$$

Note that $G(l_{\text{muscle}})$ is the potential energy of the artificial muscle when its length is $l_{\text{muscle}}$, which varies depending on the pressure applied to the muscle. When the applied pressure was set to a certain value, the function $G(l_{\text{muscle}})$ was used to determine the potential energy of the artificial muscle. By solving (8) numerically, the solutions for $r_1$, $\theta_1$, $\phi_1$, $r_2$, $\theta_2$, $\phi_2$, $h$, and $\psi$ for the applied pressure can be obtained. The MATLAB function vpasolve was used for the numerical calculations. The results of the calculation defined the deformation of the structure with respect to the applied pressure. In actual tensegrity, there is an artificial muscle of approximately 3 mm in diameter between the struts, and because the struts are 6 mm in diameter, they can only be approached up to 9 mm. Therefore, the simulation ended when the distance between the struts reached 9 mm.

Using the methods described above, simulations were conducted for all 27 placement methods for artificial muscles. However, six-bar tensegrity is a mirror image of the original structure when turned upside down; therefore, there is an artificial muscle placement method that is a mirror image of another artificial muscle placement method. For example, the arrangement of $\left(A_1^1 A_2^1,\ A_1^2 C_2^2\right)$ and $\left(A_2^2 A_1^2,\ A_2^1 C_1^1\right)$ is a mirror-image relationship. There were 10 pairs of muscle arrangements that were mirror images of each other. For the remaining seven placement methods, their mirror images are themselves. $\left(A_1^1 C_2^1,\ A_2^2 C_2^2\right)$ is an example. Therefore, the simulation results are shown only for the positive-torsion case for the 10 pairs with mirror images. The results are then shown for 17 pairs of data together with the remaining seven pairs. The simulation results for the torsion angle of the structure
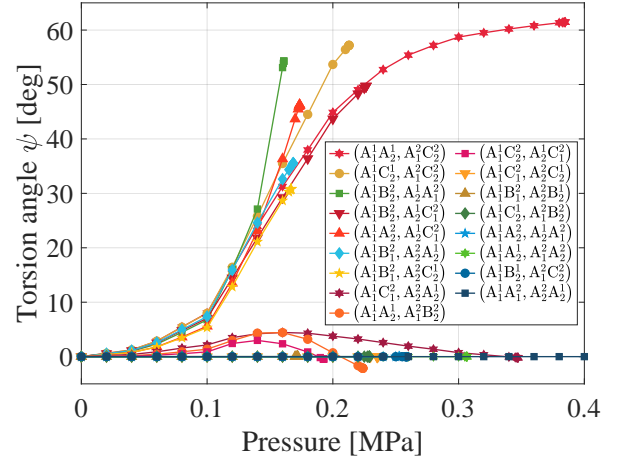


Fig. 6. The simulation result of torsion angle $\psi$ with respect to pressure applied to the artificial muscles and in all placement methods that can cause torsion. In this study, the larger torsion angle at the point of 0.4 MPa is considered superior. The data are shown up to the point where strut-to-strut contact occurred in the simulation. For those without data at 0.4 MPa, the torsional angle at strut-to-strut contact occurred was used to optimize the artificial muscles arrangement.
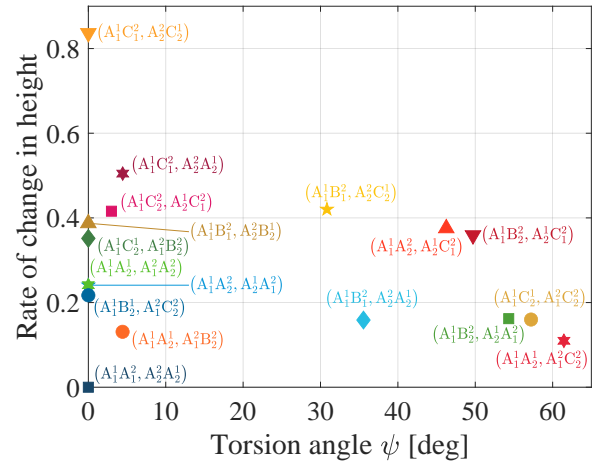


Fig. 7. The simulation result of a range of height changes relative to pressure changes, normalized by initial height with respect to the most torsion angle using all placement methods that can cause torsion. Torsion angle is desired to be large, and rate of change in height is desired to be small.

with respect to the pressure applied to the artificial muscles are shown in Fig. 6, and the rate of change of height relative to pressure change with respect to the maximum torsion angle is shown in Fig. 7.

As shown in Fig. 6, it can be seen that the placement method of the artificial muscles for the most torsion is $\left(A_1^1 A_2^1,\ A_1^2 C_2^2\right)$ which achieves 61.4 deg torsion, and the rate of change of height for this placement method is approximately 10%, as shown in Fig. 7. There are seven different artificial muscles placement methods that can torsion the tensegrity more than 30 deg, and among them, $\left(A_1^1 A_2^1,\ A_1^2 C_2^2\right)$ has the smallest rate of change in height; therefore this placement method is optimal for generating torsion in tensegrity. Hence, arrangement $\left(A_1^1 A_2^1,\ A_1^2 C_2^2\right)$ is the best in terms of both the torsional angle and height change, i.e., the smallest contraction deformation
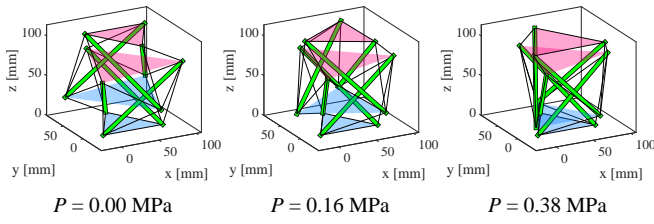
Fig. 8. Simulation results of torsional deformation of tensegrity, with artificial muscles placed in the optimal position to produce torsion $(A_1^1 A_2^1, A_1^2 C_2^2)$.
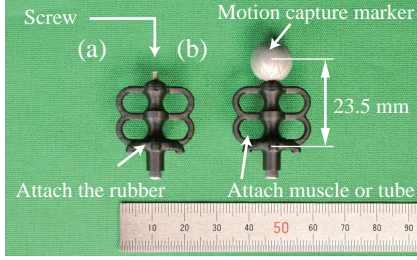


Fig. 9. Component attached to the tip of the strut to fix the artificial muscle. Since this part is hollow, a screw can be attached as shown in (a). By using the screw, a motion capture marker can be attached to the component as shown in (b).

due to torsion, and is therefore the optimal arrangement. Figure 8 shows the simulated torsional deformation of tensegrity using this arrangement. It can be seen that the triangles in the 1st and 2nd layers are twisted, as well as those in the 3rd and 4th layers, resulting in a large torsional deformation of the entire structure.

### D. Prototypes and Experiments

The optimal arrangement of artificial muscles for torsion of tensegrity obtained in the previous section has a mirror image in the form of the arrangement $(A_2^2 A_1^2, A_2^1 C_1^1)$. These two methods are applied simultaneously to a tensegrity structure to produce a tensegrity with torsions in both directions. In this case, 12 artificial muscles were attached to one tensegrity structure. In [8] pneumatic fittings which allows pneumatic pressure to be applied simultaneously to the six artificial muscles were used, and the same ones are used here.

Pneumatic pressure applied to the artificial muscle was varied from 0.0 MPa to 0.4 MPa at 0.05 MPa intervals, and the deformation of tensegrity was measured. A motion capture system was used to measure the tensegrity deformation. Figure 9 shows the apical component of the tensegrity structure. In [8], a component was attached at the end of the strut to attach the artificial muscle with rubber thread, and the component shown in Fig. 9 is a hollow version of it. By attaching a screw to this part as shown in Fig. 9(a), the top of the strut and motion capture marker can be fixed, as shown in Fig. 9(b).

Motion capture markers were attached to all the 12 vertices of the tensegrity structure, as shown in Fig. 10(A) or Fig. 10(a-c). The method for calculating the shape of the tensegrity based on this data is as follows: First, the coordinates of the tensegrity vertices were calculated from the coordinates of the motion-capture markers. The radius of the motion-capture marker was 5.5 mm, and the length of the component in Fig. 9
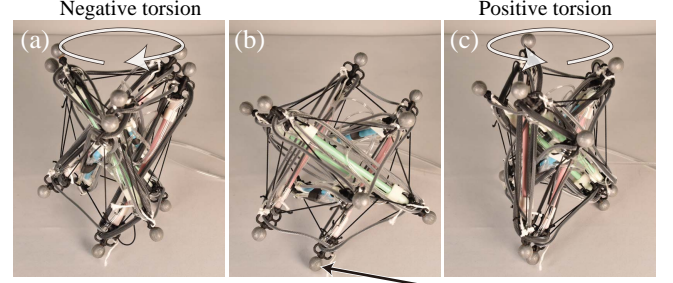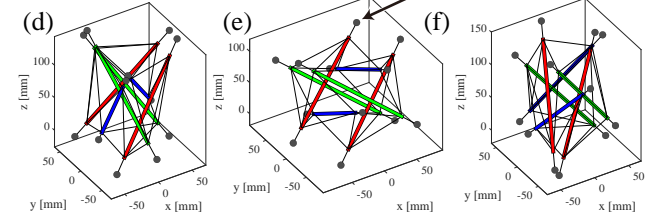


Fig. 10. (A) (i.e., (a,b,c)) The deformation in tensegrity structure. (B) (i.e., (d,e,f)) Motion capture data. (a,d) When pressure of 0.4 MPa is applied to $(A_2^2 A_1^2, A_2^1 C_1^1)$. (b,e) The initial state. (c,f) When pressure of 0.4 MPa is applied to $(A_1^1 A_2^1, A_1^2 C_2^2)$.
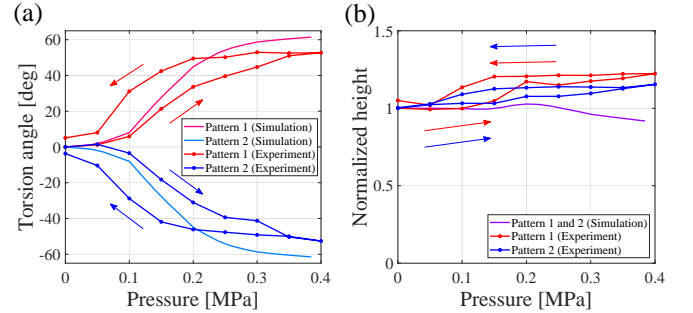


Fig. 11. Experiment result of (a) torsion angle and (b) height normalized by initial value with respect to the pressure applied to the artificial muscles.

is 18 mm. Therefore, the vertices of the structure are complemented such that each strut is shortened by 23.5 mm×2. Next, the axis $\ell$ of the tensegrity structure passing through the center of gravity of $A_1^1 B_1^1 C_1^1$ and the center of gravity of $A_2^2 B_2^2 C_2^2$ is set parallel to the z-axis by transforming the coordinates of the structure using the Rodriguez rotation formula, followed by a parallel shift to align $\ell$ and the z-axis. The height of the structure was defined as the distance between the center of gravity of $A_1^1 B_1^1 C_1^1$ and the center of gravity of $A_2^2 B_2^2 C_2^2$. Here, the orthographic projection vector $\boldsymbol{X}'$ of vector $\boldsymbol{X}$ onto the xy-plane is as follows:

$$\boldsymbol{X}' = \boldsymbol{X} - (\boldsymbol{X} \cdot \boldsymbol{e}_z) \boldsymbol{e}_z \quad (\boldsymbol{e}_z = (0, 0, 1)^\top). \qquad (10)$$

Thus, the torsion angle of the structure is defined as the average of the angles between $\boldsymbol{A}_1^{1\prime}$ and $\boldsymbol{B}_2^{2\prime}$, $\boldsymbol{B}_1^{1\prime}$ and $\boldsymbol{C}_2^{2\prime}$, and $\boldsymbol{C}_1^{1\prime}$ and $\boldsymbol{A}_2^{2\prime}$.

Using the above measurement method, the relationship between the applied pressure of the artificial muscle with the changes in the torsion angle and height of the tensegrity was obtained, as shown in Fig. 11. The change in torsion angle and normalized height were recorded while the applied pressure increased from 0.0 MPa to 0.4 MPa and then

decreased to 0.0 MPa. There was a hysteresis between the measured values and the pressure, and the arrows in Fig. 11 indicate the order of data acquisition. The $(A_1^1 A_2^1,\ A_1^2 C_2^2)$ and $(A_2^2 A_1^2,\ A_2^1 C_1^1)$ placement methods achieved a torsion of 52.7 deg and $-52.6$ deg, respectively. In the height variation, the height of the structure in the simulation decreased with increasing pressure above 0.2 MPa applied to the artificial muscle, while the height of the actual structure increased with increasing pressure. This can be attributed to the deformation in the initial state of the actual structure due to its weight and artificial muscle's deformation in radial direction, which was not accounted for in the simulation. In the simulation, the weight of the struts and artificial muscles were ignored. In the experiment, however, the structure was slightly crushed due to the influences of gravity. Therefore, the initial height of the actual structure is smaller, whereas the height when pneumatic pressure is applied is relatively higher. We also believe that volumetric interference due to the artificial muscles being inflated has a significant effect on the height deformation of tensegrity.

This experiment demonstrated that six-bar tensegrity can produce a torsional deformation of more than 100 deg while maintaining a height change of approximately 10%. Considering that the torsional deformation introduced in [21] was 4 deg in one step, it can be said that torsional deformation was achieved by an order of magnitude. In addition, torsional deformation could be achieved without losing axial softness. Furthermore, the five-stage tensegrity structure proposed in [23] torsions 20 deg per stage with a height change of 40%. Six-bar tensegrity can be considered as a two-stage tensegrity, and despite a height change of approximately 10%, a torsion of $\pm 25$ deg or 50 deg can be achieved in one stage. Therefore, the torsion angle is approximately 2.5 times larger than that in [23], indicating that the change in the height direction accompanying the torsion is exceedingly small. It was also shown that the proposed method can generate active rather than passive torsional deformation of tensegrity module.

## III. ROBOT ARM PROTOTYPING AND EXPERIMENT

This section presents an example of a tensegrity arm, which consists of tensegrity modules with several roles, and describes motion experiments to demonstrate the applicability of the large and active torsional motion of soft tensegrity proposed in this paper.

### A. Design and Development

Figure 12 shows an overall view of the created tensegrity arm. This arm consisted of four modules and the mass of the robot is 339 g. The top two modules produce large torsional deformations, Module II produces large axial contractions, and Module III is a gripping module.

Module II uses the artificial muscle placement method described in [8] as Pattern I to allow for axial contraction. Module III has the same artificial muscles arrangement as Module I, which achieves gripping motion by simultaneously activating both sets of artificial muscles for positive and negative torsions. Rubber fingers were attached to grip an
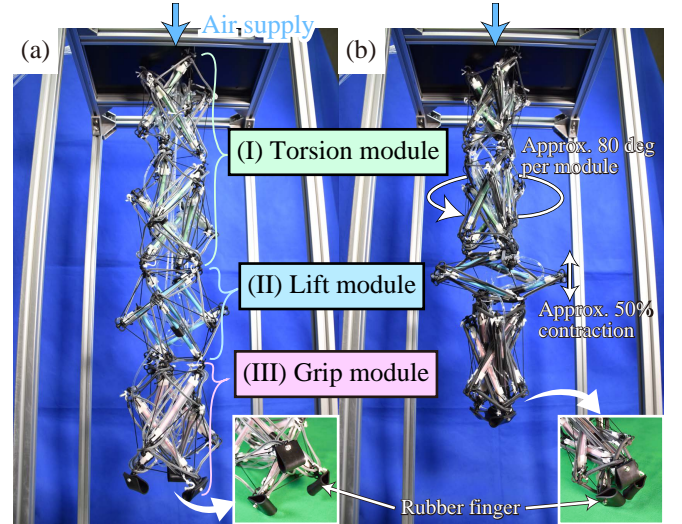


Fig. 12. Tensegrity arm consisting of two modules that can torsion, a module that can lift and a module that can grip. (a) Initial state. (b) Pressurized state.

object, as shown in Figs. 12(a) and 12(b). Figure 12(b) shows Module I for torsion, Module II for contraction, and Module III for the grip. Module I can torsion by approximately 80 deg per unit, and Module II can contract by approximately 50%.

### B. Experiment

An experiment was conducted to remove the cap of the plastic bottle using a tensegrity arm. This tensegrity arm is driven by the pneumatic system described in [8] which uses the solenoid valves. Figure 13 presents the results of this experiment. However, the cap was initially left slightly loose, and all movements were performed using only feed-forward control. First, in Fig. 13(a), Module I is negatively torsioned, Module II is uncontracted, and Module III grips the cap. By torsioning Module I in the positive direction, as shown in Fig. 13(a) to Fig. 13(b), the Module III at the end of the arm rotated approximately 160 deg and the cap was loosened. In Section II-D, each tensegrity produced 100 deg torsion, but under load, the torsion angle decreased by approximately 20 deg per module. The arm lifts with the cap released as shown in Fig. 13(c). Then, the arm returns to its negative torsion state in Fig. 13(d). This allows for the operation shown in Fig. 13(a) to Fig. 13(d) to be repeated. The actions 13(a) through 13(d) take a total of 3.5 s (0.5 s to down the arm, 1.0 s to grip the cap, 0.5 s to torsion the arm, 0.5 s to release, 0.5 s to lift the arm, and 0.5 s to torsion the arm). By lifting the arm without releasing the cap after turning it four times, the plastic bottle cap can be removed, as shown in Fig. 13(e).

## IV. CONCLUSION

This paper proposes a novel artificial muscle arrangement method. Using this method, simulations of the structural deformations were conducted for all 27 possible torsion-producing muscle configurations. Through this simulation, we found a method of placing artificial muscles that can produce $\pm 60$ deg of torsion with a single six-bar tensegrity. Furthermore, it was demonstrated that the actual structure could produce large
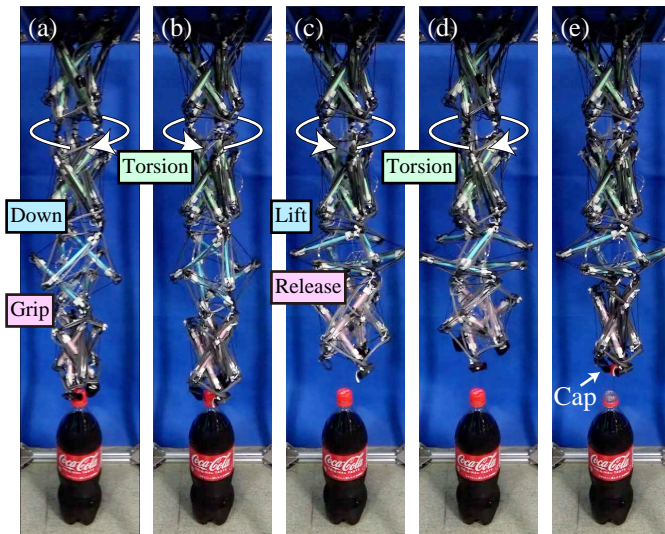
Fig. 13. (a) Module II showing arms down while Module III grips the cap. (b) Torsion the arm in the direction to loosen the cap with the Module I. (c) Module III releases the cap and Module II lifts the arm. (d) Torsion Module I back to its original state. (e) After turning the cap four times, the cap could be removed by lifting the arm without releasing the cap.

torsional deformations of $\pm 50$ deg and this is approxmately 2.5 times larger than the torsional capability of the best previous work. Torsional deformation does not cause any bending deformation, and the height change is as small as 10%; thus, it can easily be used as a module. By combining a module that can generate a large axial deformation, two modules that can generate torsional deformation, and a module that can grasp an object, a tensegrity arm was created and demonstrated the removal of a plastic bottle cap.

By integrating our previously achieved high functional tensegrity modules that can stretch [8], bend [11], and twist and combining them with sensing technology [8] for tensegrity robot shapes, we plan to develop a versatile soft tensegrity robot as shown in Fig. 1 that can operate effectively in unknown environments. Our modularized tensegrity robot will be useful for performing complex tasks in narrow spaces, which are hazardous environments for humans, while recognizing the shape of the surrounding environment.

## REFERENCES

[1] R. Buckminster Fuller, "Tensegrity," *Portfolio and Art News Annual*, vol. 4, pp. 112–127, 1961.

[2] V. Gómez Jàuregui, *Tensegrity Structures and their Application to Architecture*, ser. Books & Science. Editorial Universidad de Cantabria, 2020.

[3] K. Snelson, "The art of tensegrity," *International journal of space structures*, vol. 27, no. 2-3, pp. 71–80, 2012.

[4] T. Wang and M. A. Post, "A symmetric three degree of freedom tensegrity mechanism with dual operation modes for robot actuation," *Biomimetics*, vol. 6, no. 2, p. 30, 2021.

[5] T. Wang, M. A. Post, and A. M. Tyrrell, "Articulating resilience: Adaptive locomotion of wheeled tensegrity robot," *Electronics*, vol. 11, no. 4, p. 666, 2022.

[6] J. Rieffel and J.-B. Mouret, "Adaptive and resilient soft tensegrity robots," *Soft robotics*, vol. 5, no. 3, pp. 318–329, 2018.

[7] A. R. Barkan, A. Padmanabha, S. R. Tiemann, A. Lee, M. P. Kanter, Y. S. Agarwal, and A. M. Agogino, "Force-sensing tensegrity for investigating physical human-robot interaction in compliant robotic systems," in *2021 IEEE International Conference on Robotics and Automation (ICRA)*. IEEE, 2021, pp. 3292–3298.

[8] R. Kobayashi, H. Nabae, G. Endo, and K. Suzumori, "Soft tensegrity robot driven by thin artificial muscles for the exploration of unknown spatial configurations," *IEEE Robotics and Automation Letters*, vol. 7, no. 2, pp. 5349–5356, 2022.

[9] M. Vespignani, J. M. Friesen, V. SunSpiral, and J. Bruce, "Design of superball v2, a compliant tensegrity robot for absorbing large impacts," in *2018 IEEE/RSJ International Conference on Intelligent Robots and Systems (IROS)*, 2018, pp. 2865–2871.

[10] D. Zappetti, S. Mintchev, J. Shintake, and D. Floreano, "Bio-inspired tensegrity soft modular robots," in *Conference on Biomimetic and Biohybrid Systems*. Springer, 2017, pp. 497–508.

[11] W.-Y. Li, H. Nabae, G. Endo, and K. Suzumori, "New soft robot hand configuration with combined biotensegrity and thin artificial muscle," *IEEE Robotics and Automation Letters*, vol. 5, no. 3, pp. 4345–4351, 2020.

[12] C. Paul, F. Valero-Cuevas, and H. Lipson, "Design and control of tensegrity robots for locomotion," *IEEE Transactions on Robotics*, vol. 22, no. 5, pp. 944–957, 2006.

[13] K. Kim, A. K. Agogino, and A. M. Agogino, "Rolling locomotion of cable-driven soft spherical tensegrity robots," *Soft robotics*, vol. 7, no. 3, pp. 346–361, 2020.

[14] B. T. Mirletz, P. Bhandal, R. D. Adams, A. K. Agogino, R. D. Quinn, and V. SunSpiral, "Goal-directed cpg-based control for tensegrity spines with many degrees of freedom traversing irregular terrain," *Soft Robotics*, vol. 2, no. 4, pp. 165–176, 2015.

[15] R. L. Baines, J. W. Booth, and R. Kramer-Bottiglio, "Rolling soft membrane-driven tensegrity robots," *IEEE Robotics and Automation Letters*, vol. 5, no. 4, pp. 6567–6574, 2020.

[16] Y. Koizumi, M. Shibata, and S. Hirai, "Rolling tensegrity driven by pneumatic soft actuators," in *2012 IEEE International Conference on Robotics and Automation*, 2012, pp. 1988–1993.

[17] D. Zhou, Y. Liu, J. Deng, J. Sun, and Y. Fu, "Force enhanced multi-twisted and coiled actuator and its application in temperature self-adaptive tensegrity mechanisms," *IEEE/ASME Transactions on Mechatronics*, pp. 1–13, 2022.

[18] S. Wakimoto, K. Suzumori, and J. Takeda, "Flexible artificial muscle by bundle of mckibben fiber actuators," in *2011 IEEE/ASME International Conference on Advanced Intelligent Mechatronics (AIM)*, 2011, pp. 457–462.

[19] Y. Ushigome, R. Niiyama, K. Nishimura, T. Tanikawa, and M. Hirose, "Archi/e machina: Interactive architecture based on tensegrity," in *2010 16th International Conference on Virtual Systems and Multimedia*, 2010, pp. 55–62.

[20] T. Abe, S. Koizumi, H. Nabae, G. Endo, K. Suzumori, N. Sato, M. Adachi, and F. Takamizawa, "Fabrication of " 18 weave " muscles and their application to soft power support suit for upper limbs using thin mckibben muscle," *IEEE Robotics and Automation Letters*, vol. 4, no. 3, pp. 2532–2538, 2019.

[21] R. E. Skelton and M. C. De Oliveira, *Tensegrity systems*. Springer, 2009, vol. 1.

[22] N. Kim Pham and E. A. Peraza Hernandez, "Design exploration of a tensegrity-based twisting wing," in *International Design Engineering Technical Conferences and Computers and Information in Engineering Conference*, vol. 83990. American Society of Mechanical Engineers, 2020, p. V010T10A072.

[23] H. Lee, Y. Jang, J. K. Choe, S. Lee, H. Song, J. P. Lee, N. Lone, and J. Kim, "3d-printed programmable tensegrity for soft robotics," *Science Robotics*, vol. 5, no. 45, p. eaay9024, 2020.

[24] V. Ramadoss, K. Sagar, M. S. Ikbal, J. H. L. Calles, R. Siddaraboina, and M. Zoppi, "Hedra: A bio-inspired modular tensegrity robot with polyhedral parallel modules," in *2022 IEEE 5th International Conference on Soft Robotics (RoboSoft)*, 2022, pp. 559–564.

[25] S. Lessard, D. Castro, W. Asper, S. D. Chopra, L. B. Baltaxe-Admony, M. Teodorescu, V. SunSpiral, and A. Agogino, "A bio-inspired tensegrity manipulator with multi-dof, structurally compliant joints," in *2016 IEEE/RSJ International Conference on Intelligent Robots and Systems (IROS)*, 2016, pp. 5515–5520.

[26] S. Ikemoto, K. Tsukamoto, and Y. Yoshimitsu, "Development of a modular tensegrity robot arm capable of continuous bending," *Frontiers in Robotics and AI*, vol. 8, 2021.

[27] H. Murakami, "Static and dynamic analyses of tensegrity structures. part 1. nonlinear equations of motion," *International Journal of Solids and Structures*, vol. 38, no. 20, pp. 3599–3613, 2001.

[28] H. Murakami, "Static and dynamic analyses of tensegrity structures. part ii. quasi-static analysis," *International Journal of Solids and Structures*, vol. 38, no. 20, pp. 3615–3629, 2001.